frontiers | Frontiers in Marine Science

ORIGINAL RESEARCH
published: 10 June 2022
doi: 10.3389/fmars.2022.911492

Biotic Response to Rapid Environmental Changes During the Permian–Triassic Mass Extinction

Guoshan Li[1,2,3], Yongbiao Wang[3†], Sheng Li[3,4], Tan Wang[3], Wei Liao[5], Baozhu Deng[3] and Zhongping Lai[1]**

[1] Institute of Marine Sciences, Guangdong Provincial Key Laboratory of Marine Disaster Prediction and Prevention, Shantou University, Shantou, China, [2] Key Laboratory of Environment Change and Resources Use in Beibu Gulf (Nanning Normal University), Ministry of Education, Nanning, China, [3] School of Earth Sciences, China University of Geosciences (Wuhan), Wuhan, China, [4] No. 3 Institute of Geological and Mineral Resources Survey of Henan Geological Bureau, Zhengzhou, China, [5] Institute of Cultural Heritage, Shandong University, Qingdao, China

OPEN ACCESS

Edited by:
Fajin Chen,
Guangdong Ocean University, China

Reviewed by:
Zhicai Zhu,
Chinese Academy of Geological Sciences (CAGS), China
Hansheng Cao,
Guangdong Ocean University, China

***Correspondence:**
Guoshan Li
liguoshan@stu.edu.cn
Zhongping Lai
zhongping.lai@yahoo.com

†Deceased

Specialty section:
This article was submitted to Marine Biogeochemistry, a section of the journal Frontiers in Marine Science

Received: 02 April 2022
Accepted: 12 May 2022
Published: 10 June 2022

Citation:
Li G, Wang Y, Li S, Wang T, Liao W, Deng B and Lai Z (2022) Biotic Response to Rapid Environmental Changes During the Permian–Triassic Mass Extinction. Front. Mar. Sci. 9:911492. doi: 10.3389/fmars.2022.911492

The divergent patterns of Permian–Triassic mass extinction (PTME) have been extensively documented in varying water depth settings. We here investigated fossil assemblages and sedimentary microfacies on high-resolution samples from two adjacent sections of the South China Block: Chongyang from shallow-water platform and Chibi from deeper-water slop. At Chongyang, abundant benthos (over 80%), including rugose corals, fusulinids, calcareous algae, and large foraminifers, disappeared precipitously at the topmost of Changxing Formation grainstone, which suggested complete damage of the benthic ecosystem, confirming a sudden single-pulse extinction pattern. The end-Permian regression, marked by a karst surface, provided a plausible explanation for this extinction pattern. Whereas for the fauna in Chibi, the benthos was relatively abundant (20%–55%) with more trace fossils and lacking calcareous algae. Benthic abundance in Chibi reduced by two steps at the two claystone beds (Beds 10 and 18): bioclastic content dropped from an average of 50% in Beds 1–9 to 10% in Beds 11–17 and then to less than 5% in Beds 19–23, suggesting a two-pulse extinction. At the first pulse, large foraminifers were prominent victims in both shallow- and deeper-water settings. A plausible survival strategy for small-sized foraminifers was to migrate to deeper water to avoid extreme heat in shallow water. The early Triassic transgression prompted some small foraminifers to migrate back to original platforms and flourish briefly as disaster forms. At the Early Triassic mudstone with bottom-water settings in Chibi, the appearance of abundant small pyrite framboids (diameters of 4.74–5.96 μm), an indicator of intensified oxygen deficiency, was simultaneous with the two-step reduction of benthic diversity and abundance. Thus, anoxic conditions might be the main cause of the PTME at deeper-water settings. Our study is an example of the wider debate about biotic response to rapid environmental change for both the Permian–Triassic transition and modern days.

Keywords: Permian–Triassic mass extinction (PTME), sea-level changes, anoxic conditions, foraminiferal migration, South China Block (SCB)

1 INTRODUCTION

Mass extinctions were defined as the substantial increase in loss of taxon during a relatively short interval of geologic time, in other words, extinction rates significantly above background levels (Raup and Sepkoski, 1982; Sepkoski, 1986; Hallam and Wignall, 1997). They occurred five times in the past 600 million years (Myr) of Earth's history, known as the "Big Five," each resulting in the loss of 75%–96% of marine species biodiversity (Raup and Sepkoski, 1982; Erwin et al., 2002; Rong and Fang, 2004; Fan et al., 2020) and alteration of ecosystem structures (Aberhan and Kiessling, 2015). Current declines of biodiversity were about 1,000 times the background rate of extinction throughout geological time (Pimm et al., 2014), which may approach or exceed the magnitude of previous extinction events (Ceballos and Ehrlich, 2018). Thus, it has been suggested that Earth might be entering the sixth mass extinction (Ceballos et al., 2017; Cowie et al., 2022). While marine biodiversity decreases, the ocean system is experiencing great changes, including sea surface temperature rising (Seager et al., 2019), dissolved oxygen concentration declining (Breitburg et al., 2018), and seawater acidification (Ishida et al., 2021). The well-known Permian–Triassic mass extinction (PTME) might have been documented all these changes in modern oceans (Rong and Fang, 2004). The PTME was the severe biotic crisis of the "Big Five" (Erwin et al., 2002), resulting in the disappearance of over 80% skeletonized marine species in less than 0.03 Myr (Fan et al., 2020). Approximately >5 Myr after the crisis, the collapsed marine ecosystems did not fully recover until the beginning of the Middle Triassic (Algeo et al., 2011), indicating a significant transition in marine ecosystems from Paleozoic- to Mesozoic-type communities (Algeo et al., 2011; Song et al., 2018). Meanwhile, the terrestrial ecosystem changeover also took place nearby the Permian–Triassic boundary (PTB) (Benton and Newell, 2014; Yu et al., 2015; Zhu et al., 2020). The terrestrial ecological disturbance probably started 60,000–370,000 years before that in the ocean (Dal et al., 2022), however, the enhanced terrestrial input likely corresponding to the marine mass extinction (He et al., 2010; Benton and Newell, 2014). Nevertheless, discriminating the pattern and causes of the marine ecosystem collapse during the PTME can help us better understand the impact of rapid global warming on the ecosystems in both today and future crises.

Multiple studies on PTME have been conducted in various paleogeographical settings (e.g., Jin et al., 2000; Shen et al., 2011; Song et al., 2012; Liu et al., 2020; Li et al., 2021), but many aspects of the extinction, including its pattern and triggers, have long been disputed. Jin et al. (2000) proposed that the PTME occurred at the end-Permian as a single abrupt event based on 329 marine invertebrate species from the Meishan section in the South China Block (SCB). Yin et al. (2007) suggested a three-pulse pattern of PTME: a prelude extinction, main extinction, and the post-extinction event based on fossil records in various Permian–Triassic (P–Tr) boundary sections in the SCB. Conversely, Song et al. (2012) and Xie et al. (2005) suggested that the extinction crisis was divided into two episodic pulses from fossil records of various taxa in the Meishan section. A closer study of foraminiferal assemblage at the Liangfengya section revealed that foraminifers had two extinction pulses spanning the P–Tr boundary (Liu et al., 2020). Li et al. (2021) also found two extinction levels among benthic organisms at the Liangfengya section.

Numerous potential triggers for this crisis have been identified: rapid global warming (Sun et al., 2012), seawater anoxia/euxinia (Grice et al., 2005; Meyer et al., 2008; Hülse et al., 2021), sea-level changes (Hallam and Wignall, 1999; Ruban, 2020), and marine acidification (Payne et al., 2010; Clarkson et al., 2015). The most widely devastating mechanism was multiple environmental triggers that began with large igneous province eruptions, such as Siberian Traps (Black et al., 2012; Burgess et al., 2017; Joachimski et al., 2019; Kaiho et al., 2020), or Paleotethys ocean volcanism (Yin and Song, 2013).

However, the research on potential triggers of PTME could be affected indirectly by the uncertainty of the PTME process. Li et al. (2021) recently proposed that the two phases of PTME had different environmental triggers in the Liangfengya section. Their data confirmed that oxygen deficiency was key in the second pulse of PTME; however, the first pulse might have been triggered by other environmental factors such as high and oscillating temperatures (Sun et al., 2012) rather than an anoxia event (Isozaki, 1997; Grice et al., 2005).

Extinction patterns among benthos varied between shallow- and deep-water facies according to previous PTME investigations (e.g., Groves et al., 2005; Shen et al., 2006; Chen and Benton, 2012). To examine the intrinsic connection about various extinction patterns among environments of different water depths, we here investigated the lithologic succession and benthonic assemblages from Late Permian to Early Triassic in two adjoining sections. We further discussed the extinction patterns, possible environmental triggers, and survival mechanisms during the PTME. This investigation of biotic response to rapid environmental changes can help us better understand the extinction and survival process, including modern-day global environmental disasters.

2 Paleogeography and Sedimentary Background

During the Late Permian to the Early Triassic, the SCB was located near the paleoequator, in the eastern Paleotethys Ocean, where the shallow-water Yangtze Platform was separated by several deep-water siliciclastic basins (**Figure 1**). In the past two decades, attention was focused on the sedimentary successions in SCB. The huge exposures, length of the sections, and improved chronology provided a good opportunity to track environmental changes and restoration of benthic ecosystems during the P–Tr transition.

Abbreviations: BSE, backscattered electron; GSSP, Global Stratotype Section and Point; MEH, mass extinction horizon; MU, microbialite unit; OMZ, oxygen minimum zone; PTB, Permian–Triassic boundary; PTME, Permian–Triassic mass extinction; SCB, South China Block; SEM, scanning electron microscopy; SMF, standard microfacies.

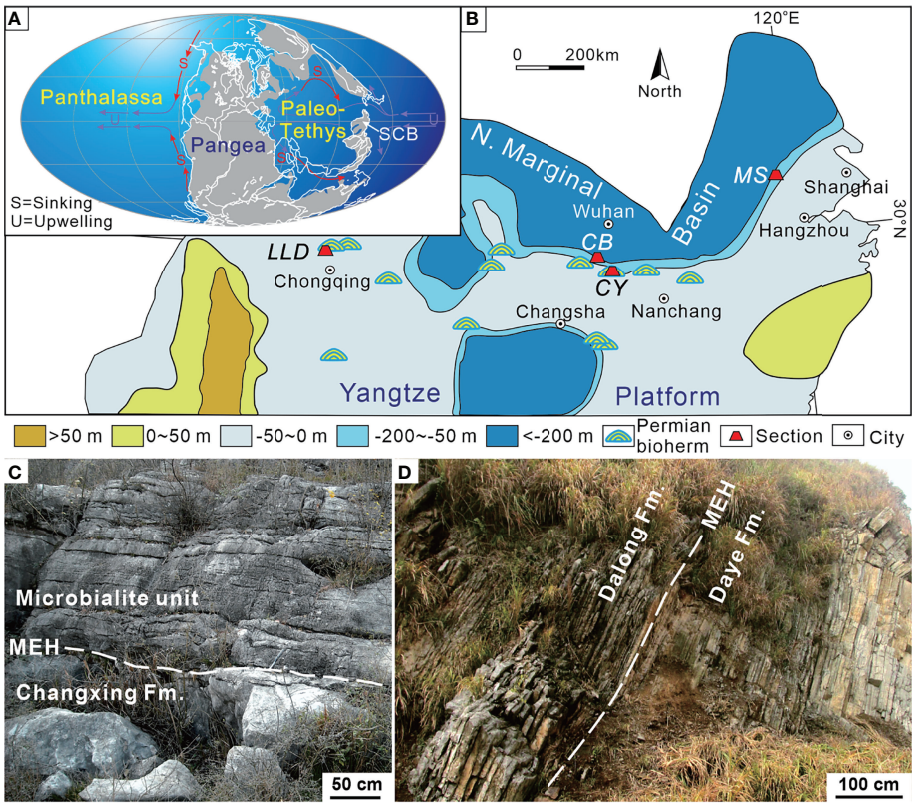

FIGURE 1 | Changhsingian paleogeographic map showing the location of the sections investigated. **(A)** Global map revised from Scotese (2001). **(B)** Base map of the South China Block revised from Wang and Jin (2000). **(C)** Field outcrop of the Chongyang section showing the lower part of the microbialite unit and Late Permian grainstone near the P–Tr boundary. **(D)** Field outcrop of the Chibi section in Xianning city showing the P–Tr transition sequence. MEH, mass extinction horizon; SCB, South China Block; *CB*, Chibi section; *CY*, Chongyang section; *LLD*, Laolongdong section; *MS*, Meishan section.

2.1 The Chongyang Section

The Chongyang section (114°20′16″E, 29°39′08″N), located at Dashi village of Chongyang County southeast of Hubei Province (**Figure 1B**), has been described by Wang et al. (2005). The P–Tr boundary successions are well exposed, making it easy to identify the mass extinction horizon (MEH) (**Figure 1C**). On the outcrop, the coral reef framestone and skeletal grainstone are visible in the lower part of the section (Yang et al., 2011), yielding foraminifera *Palaeofusulina sinensis*. The skeletal grainstone under the MEH is Late Permian in age on the basis of *Palaeofusulina*. The Late Permian grainstone contains more than 80% (relative to the sediments) fossils, including rugose corals, fusulinids, calcareous algae, foraminifers, crinoids, bryozoans, brachiopods, and several other metazoan fossils. On the top of the skeletal grainstone is now an undulating paleokarst surface, capped with weathering and erosion residual products (Wang et al., 2019). The paleokarst surface formed widely at the shallow platform of the SCB (Ezaki et al., 2003; Wu et al., 2010; Kershaw et al., 2012) due to its exposure by the end-Permian regression (Yin et al., 2014). The overlying microbialite unit (MU) is characterized by thrombolite and dendrolite, which differ distinctly from Late Permian skeletal grainstones. Yang et al. (2006) elucidated the composition and structure of microbialite ecosystems in the Chongyang section following the PTME. The MU lies on Permian skeletal grainstones and is overlain by thin-bedded micrites up to 8.5 m thick (**Figure 2**). The upper part of MU has several layers of molluskan grainstone. There is a regression hiatus between the Upper Permian Changxing Formation and the MU (Yin et al., 2014).

Despite the fact that conodont fossils such as *Hindeodus parvus*, *Hindeodus typicalis*, and *Hindeodus latidentatus* had been found in the middle MU (Yang et al., 2006), more comprehensive work from various sections indicated that conodont fossil *H. parvus* was actually preserved at the bottom of the MU (Jiang et al., 2014; Wang et al., 2016). Therefore, the P–Tr boundary in the Chogyang section was allocated to the bottom of the MU in this study, and the MU was assigned to the *H. parvus* Zone (Jiang et al., 2014; Wang et al., 2016).

2.2 The Chibi Section

The Chibi section (113°49′13″E, 29°42′01″N) is located at Fenghuang Mountain in southeast Hubei Province. This section is positioned in the transitional zone between the Yangtze Platform and the northern marginal deep siliceous

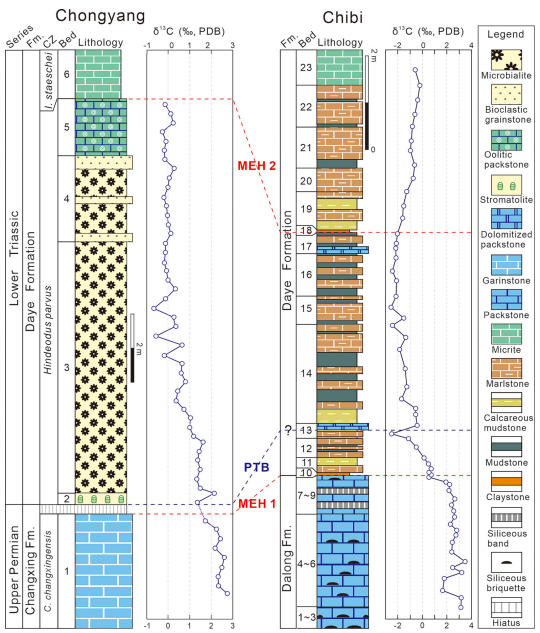

FIGURE 2 | Columnar sections of P–Tr successions of the Chongyang and Chibi sections. Conodont zonation of the Chongyang section from Yang et al. (2006) and Wang et al. (2019). The δ^{13}Ccarb of the Chongyang section from Wang et al. (2019). CZ, conodont zones; *C.*, *Clarkina*; *I.*, *Isarcicella*; MEH, mass extinction horizon; PTB, P–Tr boundary.

basin during the P–Tr transition (**Figure 1**; Feng et al., 1996). A deep siliciclastic deposition exists in the northern area to Chibi, such as Daye or Huangshi (Wang and Xia, 2003). The southern area consists of a shallow-water carbonate platform (Liu et al., 2010).

The particular paleogeographic setting resulted in the formation of a distinct sedimentary sequence within the P–Tr interval (**Figure 2**). The Upper Permian Dalong Formation (Beds 1–9) is characterized primarily by a sequence of thin- to medium-bedded bioclastic packstones interlayered with a small amount of siliceous thin beds. Packstones contain benthic fossils, such as foraminifers, calcareous algae, and echinoderms. The PTME occurred at the base of the first claystone (Bed 10), where a diversified benthic assemblage disappeared, which was dominated by small foraminifers and calcareous algae (Deng et al., 2015). Numerous siliceous beds had accumulated during the first MEH (MEH 1) in the Dalong Formation, indicating increased volcanism (Wang et al., 2019). The fine-grained lithologies of the overlying Daye Formation include micrites, marls, mudstones, and claystones, with sparse bivalves and ammonoids. Abundant small pyrite framboids in Beds 11–21 suggested a low oxygen level in bottom waters (Wignall and Hallam, 1996).

Although no identifiable conodont had been found to confirm the P–Tr boundary of the Chibi section, the Bed 25 "boundary clay" of the Meishan section, known as the Global Stratotype Section and Point (GSSP) for the P–Tr boundary (Yin et al., 2001), had been considered to be a reliable marker of P–Tr boundary (Peng and Tong, 1999). Bed 10 of the Chibi section can be compared to it based on the first appearance of the basal Triassic marker, the bivalve *Claraia wangi* (in Bed 17), *C. stachei* (in Bed 21), and the ammonoid *Hypophiceras* (in Bed 18) (**Figure 3**). Based on biostratigraphy, a large excursion of carbon isotope is a useful indicator of stratigraphic correlation (Song et al., 2012). The first negative shift was recorded at Bed 13 and a weaker positive shift is recorded at the lower part of Bed 14 of the Chibi section (**Figure 2**). Thus, the P–Tr boundary is located in the middle of Bed 13 (i.e., 94 cm above the first claystone of the Daye Formation base).

3 METHODS

3.1 Fossil Assemblage

Bioclastic was investigated under the microscope to examine the taxonomic composition of fossils. In each sample, calcareous algae, fusulinids, non-fusulinid foraminifers, bivalves, gastropods, ostracods, echinoderms, and microbes were classified according to guidelines of Flügel (2004). The changes of these fossil groups were recorded across the P–Tr boundary in the carbonate platform. A quantitative statistical method that was introduced by Payne et al. (2006) for bioclastic grains, i.e., a Figure of 500 points (or 300 points in some cases) was chosen to determine the contents of bioclastic grains, with an error of ±2.5% (Wen and Liu, 2009).

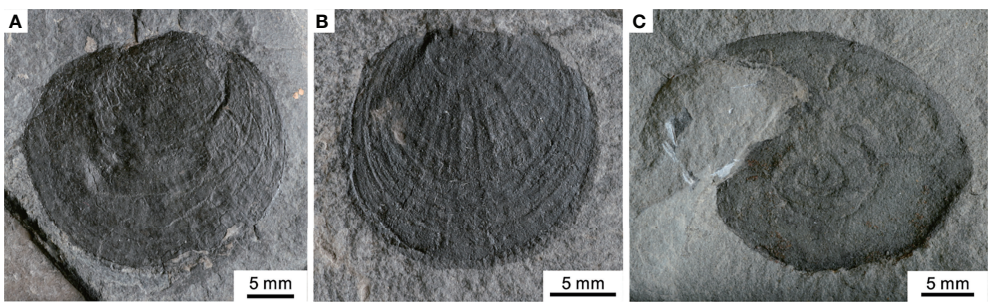

FIGURE 3 | The Early Triassic marker, bivalves and ammonoids of the Chibi section. **(A)** *Claraia wangi* from Bed 17. **(B)** *Claraia stachei* from Bed 21. **(C)** *Hypophiceras* sp. from Bed 18.

3.2 Microfacies Analysis

The analysis of carbonate microfacies was carried out according to standardized microfacies (SMF) and the depositional pattern (Flügel, 2004), focusing on fossil fragments and lithologic characters from both outcrops and thin sections. During the fieldwork, macrofossils, lithologic characters, and sedimentary structures were observed on outcrops. Small fossil fragments and other microlithologic characters in thin sections were examined under a polarizing microscope. The content of fossil fragments was calculated using the methodology by Payne et al. (2006).

3.3 Pyrite Framboid Analysis

Thirty vertically oriented samples with ca. 2 × 2 cm^2 in size across the P–Tr boundary in the Chibi section were selected to analyze size distributions of pyrite framboid for the study of redox conditions. Three samples from packstone of the Upper Permian Dalong Formation, 18 from the thin-bedded mudstone/marlstone of the P–Tr "transitional beds," and five from the Lower Triassic Daye Formation were investigated. Initially, each sample was polished for petrographic observation under a microscope. Pyrite framboids of each polished sample were measured *in situ* using an FEI Quanta 200 scanning electron microscope (SEM). A minimum of 120 pyrite framboids were measured for each sample wherever appropriate: this quantity was considered sufficient for the statistical analysis with an error less than 10% (Wilkin et al., 1996).

4 RESULTS

4.1 Fossil Assemblage and Microfacies of the End-Permian

The sedimentary sequence at the Chongyang section starts with gray thick-bedded bioclastic grainstones belonging to the Upper Permian Changxing Formation, yielding foraminifer *Palaeofusulina sinensis*. Thin-section data revealed that the Changxing Formation was mostly made up of skeletal grainstones cemented by sparite calcite, and that calcareous algae, fusulinids, non-fusulinida foraminifera, ostracods, gastropods, coral, bryozoan, and echinoderms were well-preserved fossil grains (**Figure 4A**). The biotic abundance was extremely high with an average of 66% (**Figure 4B**) and could come out >80% in some samples, implying a turbulent shallow-water platform environment. Furthermore, a number of fusulinids were identified in thin sections (**Figure 5**), indicating that the water depth was about 20–30 m (Yu, 1989). The foraminiferal assemblage was similar to those examined on shallow-water platforms elsewhere in the SCB, where *Reichelina*, *Cribrogenerina*, and *Palaeofusulina* were commonly abundant (Yang et al., 2011). The cement was largely composed of sparite and contained no micrite, indicating a high water-energy content. The presence of abundant algae and coral indicated that the seafloor was within the euphotic zone (**Figure 4A**). The diverse benthic community preserved in the Permian bioclastic grainstone of the Chongyang section indicates a well-oxygenated water column (Groves et al., 2005).

Microfacies type of Bed 1 was diagnosed in comparison with SMF, which was similar to SMF 18 (Flügel, 2004). According to the sedimentary model (Flügel, 2004), the Chongyang section was located in a typical shallow-marine carbonate platform environment with relatively high water-energy during the Late Permian Changhsingian.

The sedimentary sequence of the P–Tr interval at the Chibi section started with a dark gray thin-bedded bioclastic packstone with siliceous interbeds belonging to the Upper Permian Dalong Formation. The Dalong Formation was mainly composed of bioclastic packstone cemented by sparite calcite according to thin section (**Figure 6A**). Well-preserved fossils, such as calcareous algae, fusulinida, non-fusulinida foraminifera, and gastropods, had easily identified taxonomic traits and a weak orientation. The diversity was moderate, and the biotic abundance was relatively high, ranging from 20% to 55% (**Figure 6B**). These foraminifera fragments, such as *Reichelina*, *Earlandia*, and *Diplosphaerina*, have small particle sizes, ranging from 100 to 200 μm (**Figure 7**).

The Chibi section was dominated by benthos, in contrast to the typical deep-water silicalite basin characterized by planktonic radiolarian fossils (Meng et al., 2014). Those benthos were

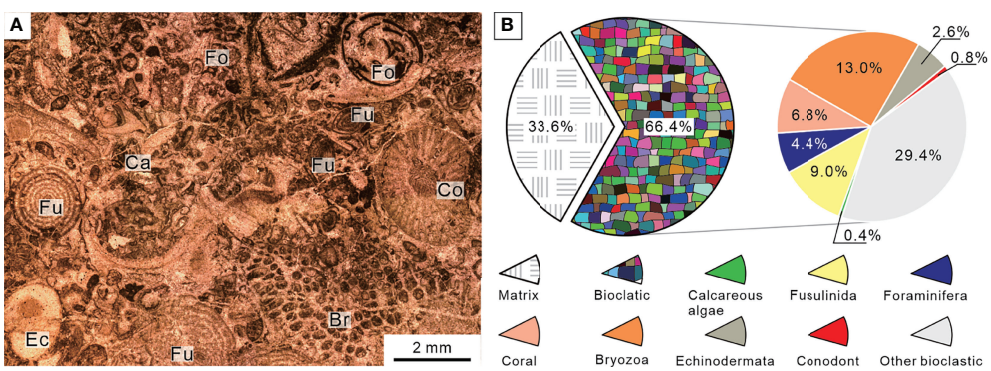

FIGURE 4 | Micropetrologic characters **(A)** and percentages of fossil assemblages **(B)** of bioclastic grainstones from Bed 1 in the Chongyang section before the PTME. Br, Bryozoa; Ca, Calcareous algae; Co, Coral; Ec, Echinodermata; Fo, Non-fusulinida foraminifera; Fu, Fusulinida.

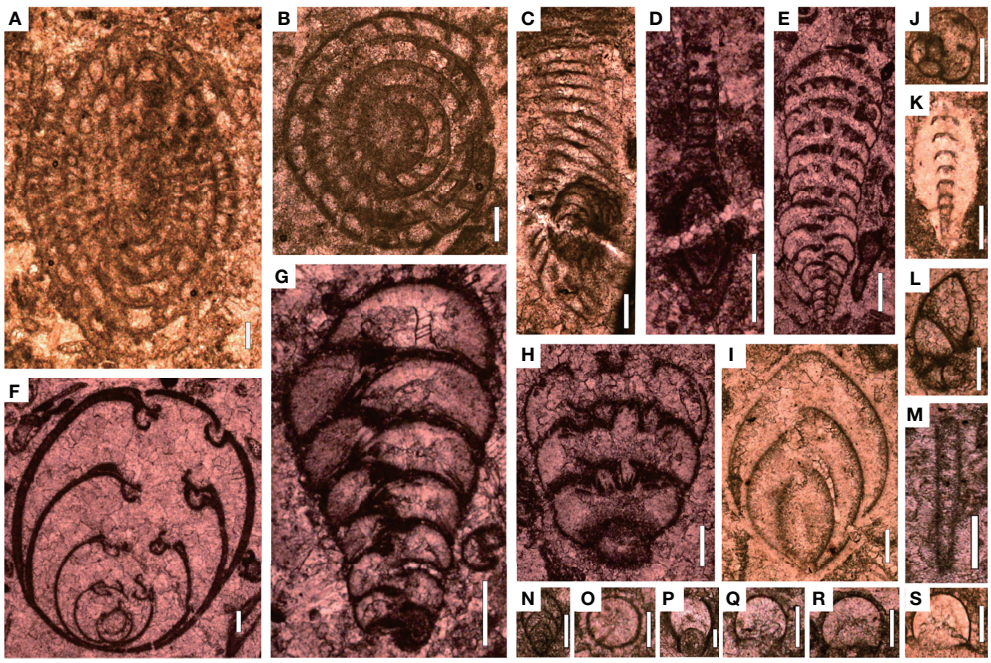

FIGURE 5 | Foraminifers from Bed 1 of the Chongyang section before the PTME. **(A)** Nankinella orientalis; **(B)** Sphaerulina crassispira; **(C)** Reichelina purlchra; **(D)** Reichelina media; **(E)** Climacannina spathulata; **(F)** Paraglobivalvulina piyasini; **(G)** Palaeotextularia longiseptata; **(H)** Cribrogenerina prosphaerica; **(I)** Ichthyofrondina palmata; **(J)** Poatendthyrasp.; **(K)** Pachyphloia ovata; **(L)** Globivalvulina sp.; **(M)** Earlandia sp.; **(N)** Frondina permica; **(O–S)** Diplosphaerna inaequalis. Scale bars in panels **(A–I)** are 200 μm in length and in panels **(J–S)** are 100 μm.

different from that of the Chongyang section, which is a typical shallow platform section in the Late Permian with a lower diversity. A few broken fragments of calcareous algae were found in thin sections (**Figure 6A**), which might have originated from the southern carbonate platform in shallower water (Deng et al., 2015). The cement was mainly composed of micrites and few sparites, indicating that water-energy was relatively low. Therefore, this microfacies resembles SMF 5 (Flügel, 2004). We inferred that the Chibi section was located at the bathyal outer slope between the shallow-water platform and the deep-water basin, slightly deeper than Meishan, during the end-Permian.

Multiple trace fossils were found in the bioclastic wackestone of Bed 6, about 2 m below the MEH 1 (**Figure 8**). The majority of these trace fossils were burrows several centimeters long. The abundance of burrows indicated that the seafloor was suitable for the life of benthic surface organisms and benthic endophytic burrowing organisms (Chen et al., 2015). The microfacies belong to SMF 9-BIOTRUB "burrowed bioclastic wackestone," which was found on the deep-water shelf (Flügel, 2004). Considering a

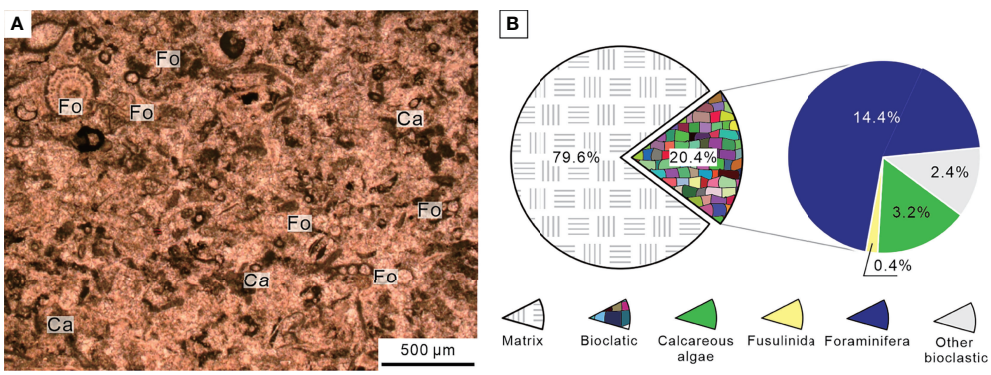

FIGURE 6 | Micropetrologic characters **(A)** and percentages of fossil assemblages **(B)** of bioclastic packstone from Bed 5 in the Chibi section before the PTME. Ca, Calcareous algae; Fo, Non-fusulinida foraminifera.

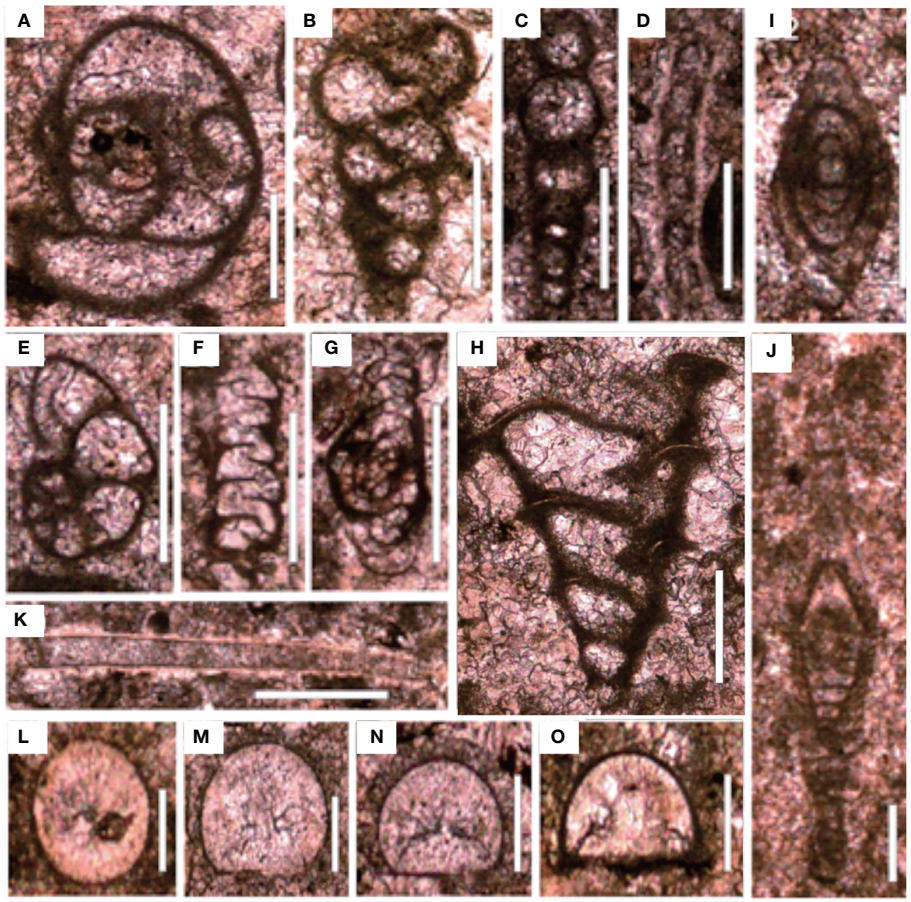

FIGURE 7 | Foraminifers from the Chibi section before the PTME. **(A)** Poatendothyra tenuis; **(B)** Dagmarita sp.; **(C)** Nodoinelloides neischajewi; **(D)** Rectocornuspira kalhori; **(E)** Globivalvulina sp.; **(F)** Ammovertella sp.; **(G)** Hemigordius sp.; **(H)** Dagmarita chanakchiensis; **(I)** Reichelina changhsingensis; **(J)** Reichelina matsushitai; **(K)** Earlandia sp.; **(L–O)** Diplosphaerina inarqualis. Scale bars in panels **(A–K)** are 100 μm in length and in panels **(L–O)** are 50 μm.

few broken algae fragments and fecal pellets, we proposed that the seafloor should be below the photic zone with a water depth of 100–200 m.

4.2 Fossil Assemblage and Microfacies During the Permian–Triassic Interval

Microbialites dominated the shallow platform of the SCB during the Early Triassic transgression directly after the end-Permian regression, representing a disaster biota due to the lack of skeletal organisms (Wang et al., 2005). The MU comprised a series of microbialite forms in the Chongyang section (Wang et al., 2019). Numerous metazoan fossils were found within the MU, including small foraminifera, microgastropods, and ostracods (Yang et al., 2011), all of which exhibited varying and had low diversity. One remarkable feature of microbialite is well-preserved calcified cyanobacteria (**Figure 9A**), reflecting an absence of metazoan predation. The microfacies was similar to that of SMF 21 (Flügel, 2004). The microfacies of Bed 2 belong to SMF 21-PORO, which was formed in very shallow supratidal environments, such as restricted or evaporitic lagoons. The microfacies of Beds 3 and 4 belong to SMF 21-PORO, which was formed mostly in shallow subtidal or intertidal environments.

Following the thrombolite disappearance, an oolitic packstone was deposited. These packstones consisted of poorly sorted ooids within the micrite matrix (**Figure 9B**). The rapid transition from thrombolite facies to an oolitic facies indicated a significant change in the marine environment. Majority of modern marine ooids are found in warm waters and wave/current churned settings (Diaz et al., 2015), such as the Great Bahama Bank (Harris et al., 2019), while poorly sorted ooids are in more tranquil environments (O'Reilly et al., 2017). The microfacies were similar to that of SMF 15 (Flügel, 2004). Modern stromatolites were reported mainly in Shark Bay and Bahamas in middle America, where the most prevalent water depths range from intertidal to 10 m (Chivas et al., 1990; Reid et al., 1995). We infer that this type of microfacies was formed in a relatively low water-energy environment along the platform margin and was the result of further deepening in the water depth during the Early Triassic transgression (Kershaw et al., 2012).

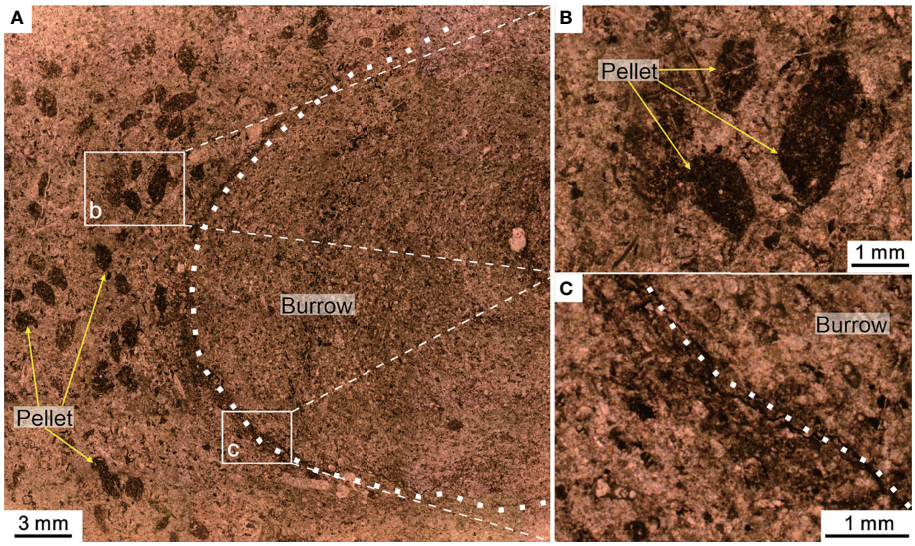

FIGURE 8 | Trace fossil (burrow) and fecal pellets from Bed 6 of the Chibi section before the PTME. **(A)** The cross-section of a burrow and the well-demarcated boundary (dotted line). Panels **(B, C)** are the magnified images from the two white boxes in panel **(A)**.

The lower part of Daye Formation (Beds 11–14) comprised dark thin-bedded fine-grained lithologies, including micrites, marls, mudstones, and claystones on outcrops. Bioclastic content was found to be very low, ca. 5%~10%, with a few small foraminifers, echinoderms, gastropods, and ostracods in thin sections (**Figure 10A**). Small pyrite framboids were relatively common. The microfacies was similar to SMF 8 (Flügel, 2004). This microfacies is common both in the deep open shelf and in shallow lagoons. The micritic matrix indicated a restricted low-energy environment. Thus, we inferred that the microfacies formed in tranquil subtidal facies. However, some echinoderm and small gastropod fragments occasionally have been found in Beds 15–17 (**Figure 10B**). Bioclastic content was higher than 25% and mainly composed of small gastropods and ostracods. This microfacies belonged to SMF 8 (Flügel, 2004). Accordingly, we inferred that this microfacies was formed in the deep shelf with a low water-energy, standing for the subtidal facies.

4.3 Fossil Assemblage and Microfacies of the Early Triassic

The topmost of the Chongyang section (Bed 6) comprised of gray medium- to thick-bedded micrites on outcrop. Rare fossil fragments were observed in thin sections under the microscope, but pyrite framboids were relatively common (**Figure 11A**). The microfacies was similar to that of SMF 9 (Flügel, 2004). For the micritic matrix and the lack of fossils, we inferred that this type of

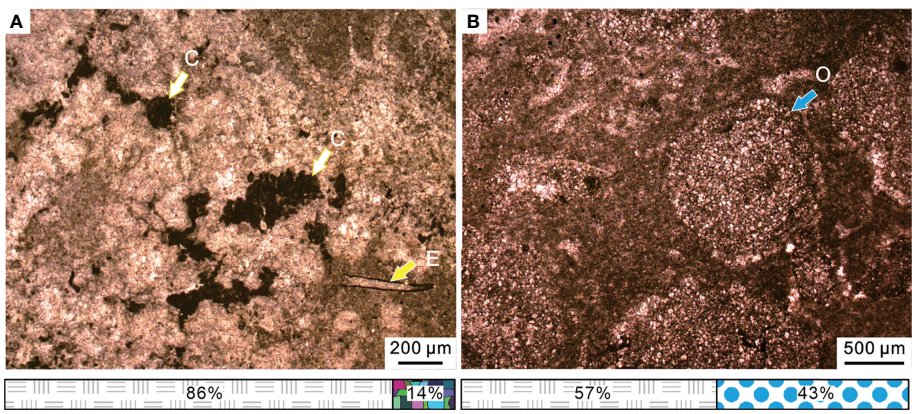

FIGURE 9 | **(A)** Spherical calcified cyanobacteria and small foraminifera *Earlandia* sp. of the microbialite from Bed 3 in the Chongyang section. **(B)** Micropetrologic characters of Bed 5 in the Chongyang section, including poorly sorted ooids within the micrite matrix. The legend is consistent with that of **Figure 4**. C, cyanobacteria; E, *Earlandia* sp.; O, ooids.

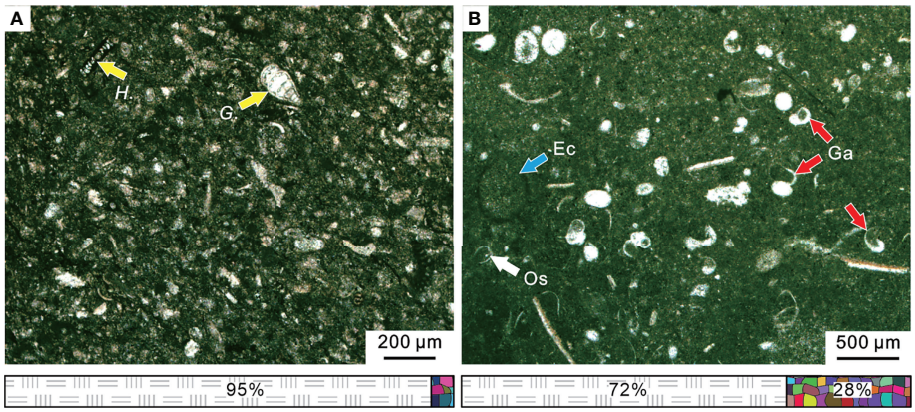

FIGURE 10 | Micropetrologic characters and fossil assemblages of micrites in the Chibi section during the PTME interval. **(A)** From Bed 11. **(B)** From Bed 15. The legend is consistent with that of **Figure 4**. Ec, Echinoderm; Ga, gastropod; Os, ostracod; *G.*, *Geinitzina*sp.; *H.*, *Hemigordius* spp. The legend is consistent with that of **Figure 4**.

microfacies was formed in restricted lagoons with a low water-energy.

Above the MEH 2, the Early Triassic stratigraphic succession of the Chibi section was mainly characterized by black mudstones with a gray-black marlstone interlayer that expanded with transgression and increased water depth. The abundance of bivalves found in field outcrop varied but showed low diversity. No benthic community was found in field outcrops or thin sections (**Figure 11B**). The microfacies was similar to SMF 9-L, which was located near the bottom of the slope or deep-water shelf (Flügel, 2004).

4.4 Pyrite Framboid Size Distributions in the Chibi Section

Out of the 26 samples, two samples from Dalong Formation had no pyrite framboids, while one (sample LFY -16) had a trace amount of pyrite framboids or authigenic crystals. However, backscattered electron (BSE) images revealed that 23 samples from the Daye Formation were generally rich in pyrite framboids (except sample LFY +379) (**Figure 12A**). A plot of mean diameter and standard deviation of pyrite framboid is shown in **Figure 12B** for the purpose of paleoredox interpretation. The parameters of size distribution are summarized in **Table 1**.

We collected 18 samples from the P–Tr transition beds (Beds 10–17) and measured 3,730 pyrite framboids (more than 200 framboids per sample) (**Table 1**). The majority of pyrite framboids were less than 10 μm. The mean diameters of the 18 samples varied from 4.08 ± 1.07 μm to 11.77 ± 4.90 μm, suggesting that the oxygen levels of bottom water fluctuated between upper dysoxia and anoxia during the P–Tr transition interval. We collected five samples from Beds 19–21 and measured 974 pyrite framboids (ca. 195 framboids per sample) (**Table 1**). These five samples had a mean diameter range of 4.74 ± 1.46 μm to 5.96 ± 1.67 μm, indicating that the bottom water at the Chibi site had a stable reduced oxygen environment (Bond and Wignall, 2010).

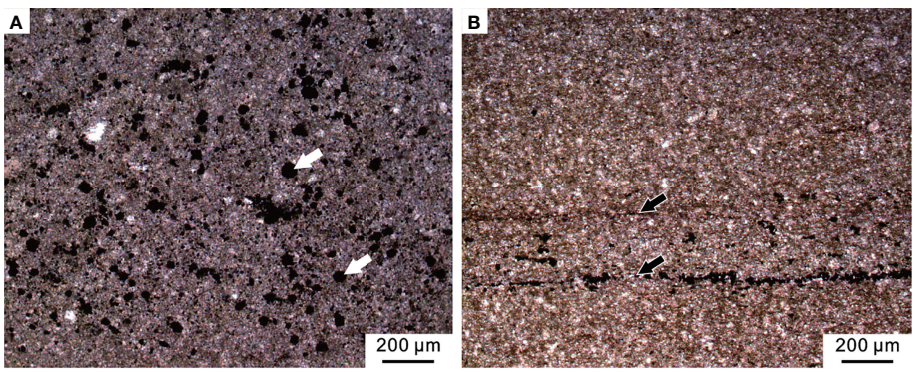

FIGURE 11 | Micropetrologic characters after the PTME. **(A)** Micrite from Bed 6 of the Chongyang section bearing abundant pyrite framboids (white arrows). **(B)** Mudstone from Bed 19 of the Chibi section, including organic laminas (black arrows).

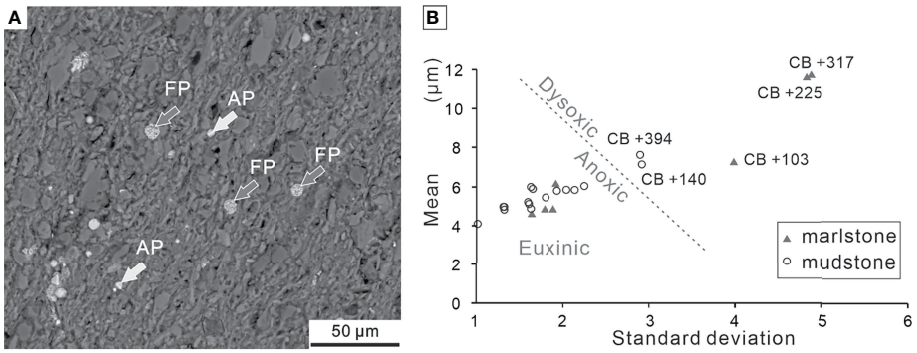

FIGURE 12 | **(A)** Overview of BSE images of framboidal pyrites and authigenic pyrites from Bed 19 of the Chibi section. **(B)** Cross-plot of mean diameter vs. standard deviation of pyrite framboids from the Chibi section. The boundary (dotted line) separating dysoxic and anoxic/euxinic fields is from Bond and Wignall (2010). FP, framboidal pyrites; AP, authigenic pyrites.

TABLE 1 | Pyrite sample parameters observed from the Chibi section.

Bed No.	Sample level (cm)	Lithology	Number of framboids measured	Minimum framboid diameter (μm)	Maximum framboid diameter (μm)	Mean framboid diameter (μm)	Standard deviation of framboid diameter	Median framboid diameter (μm)	Inferred redox conditions
21	+678	Mudstone	196	1.98	10.25	4.74	1.46	4.42	Anoxic
19	+606	Mudstone	178	2.23	12.14	5.84	2.03	5.39	Anoxic
	+574	Mudstone	201	2.07	12.18	5.96	1.67	5.86	Anoxic
	+548	Mudstone	208	2.29	9.38	4.94	1.36	4.71	Anoxic
	+525	Mudstone	191	2.66	11.02	5.91	1.70	5.60	Anoxic
17	+499	Mudstone	199	2.35	10.77	4.98	1.37	4.95	Anoxic
	+488	Mudstone	229	1.98	9.23	4.81	1.37	4.71	Anoxic
16	+468	Mudstone	185	2.11	10.34	5.20	1.64	4.87	Anoxic
	+453	Mudstone	183	2.03	13.56	6.03	2.30	5.56	Anoxic
	+394	Mudstone	177	2.44	15.73	7.66	2.94	7.21	Dysoxic
15	+379	Marlstone	63	2.24	11.06	6.17	1.97	6.10	Dysoxic
	+363	Mudstone	157	2.66	12.76	5.87	2.09	5.26	Anoxic
	+347	Mudstone	248	2.04	8.82	4.08	1.07	3.87	Anoxic
	+317	Marlstone	119	3.88	25.97	11.77	4.90	10.47	Dysoxic
14	+265	Mudstone	312	1.73	15.20	5.83	2.19	5.35	Anoxic
	+233	Mudstone	260	2.34	11.23	5.10	1.65	5.10	Anoxic
	+225	Marlstone	149	3.85	25.19	11.56	4.85	10.53	Dysoxic
	+185	Mudstone	262	2.29	11.29	5.43	1.85	5.09	Anoxic
	+140	Mudstone	281	1.82	16.35	7.16	2.96	6.47	Dysoxic
13	+103	Marlstone	266	2.41	22.32	7.30	4.01	6.15	Dysoxic
	+74	Marlstone	147	2.21	10.53	4.86	1.93	4.32	Anoxic
11	+35	Marlstone	254	1.76	11.87	4.86	1.83	4.53	Anoxic
	+12	Marlstone	239	1.76	10.87	4.62	1.68	4.19	Anoxic
9	-16	Limestone	8	5.10	10.25	#	#	#	Oxic
8	-34	Limestone	#	#	#	#	#	#	Oxic
	-53	Limestone	#	#	#	#	#	#	Oxic

Sample level "-53" means 53 cm below the first mass extinction horizon (MEH 1), and "+678" means 678 cm above the MEH 1. "#" means no data.

5 DISCUSSION

5.1 Single Abrupt Extinction Pulse in the Platform Setting

The PTME pattern has been debated for several decades (e.g., Stanley and Yang, 1994; Jin et al., 2000; Shen et al., 2011; Song et al., 2012; Dal et al., 2020). Investigations have revealed a complex process of the PTME. Among different benthos, on the one hand, the extinction patterns and magnitudes were varied: extinctions among foraminifers occurred as a one-pulse extinction pattern (Groves et al., 2005), whereas ostracods exhibited two extinction pulses (Forel, 2013; Wan et al., 2019). On the other hand, among different paleogeographic settings, sharply different patterns of the same faunas had also been observed, typified by foraminiferal extinction (Song et al., 2009; Zhang and Gu, 2015; Li et al., 2021).

The stratigraphic succession from the end-Permian to Early Triassic interval in the Chongyang section was very clear at the outcrop. The top of the Changxing Formation grainstones was coated by residual deposits enriched in ferric oxide, quartz, and

feldspar, which probably represented the weathering and erosion products following its exposure by the end-Permian regression (Wu et al., 2006). The overlying lower part of the Daye Formation was dominated by MU, indicating a dramatic change in the marine ecosystem from end-Permian to Early Triassic. The MEH was located topmost of the Changxing Formation grainstones.

The Upper Permian Changxing Formation in the Chongyang section was characterized by the deposition of reef framestone and grainstone enriched in diverse benthos, such as corals, calcareous algae, echinoderms, and foraminifers under the microscope (**Figure 13I**). However, most benthos such as rugose corals, fusulinida, calcareous algae, and large foraminifers disappeared in the topmost of the Changxing Formation grainstone. Small foraminifers, such as *Diplosphaerina inaequalis* and *Earlandia* sp., survived during this extinction pulse (**Figure 13H**) but eventually disappeared quickly (**Figure 13G**). The bioclastic abundance dropped to less than 15% (**Figure 9**), down from 66% or higher than this value in the Changxing Formation grainstones (**Figure 4**).

The pattern indicated a sudden extinction at the base of the MU in the Chongyang section. The abrupt extinction process had been documented in various shallow water settings of the Pangea (Groves et al., 2007; Angiolini et al., 2010). Foster et al. (2019) proposed that a shallow microbialite could provide a "refuge" for some marine invertebrates during mass extinction, where disaster forms could create a unique and ephemeral ecosystem. Significant disaster forms, such as ostracods, small gastropods, tubeworms, and brachiopods, bloomed ephemerally and formed a stratiform bioclastic grainstone in the MU of the Chongyang section (**Figure 14**). In summary, the Chongyang section from the shallow platform suffered an abrupt extinction pulse, resulting in a crashed ecosystem structure.

5.2 Two-Pulse Extinction in Slope Setting

However, compared to the Chongyang section, the benthos of the Chibi section, which was located on the outer slope, did not completely disappear after the first PTME pulse. The

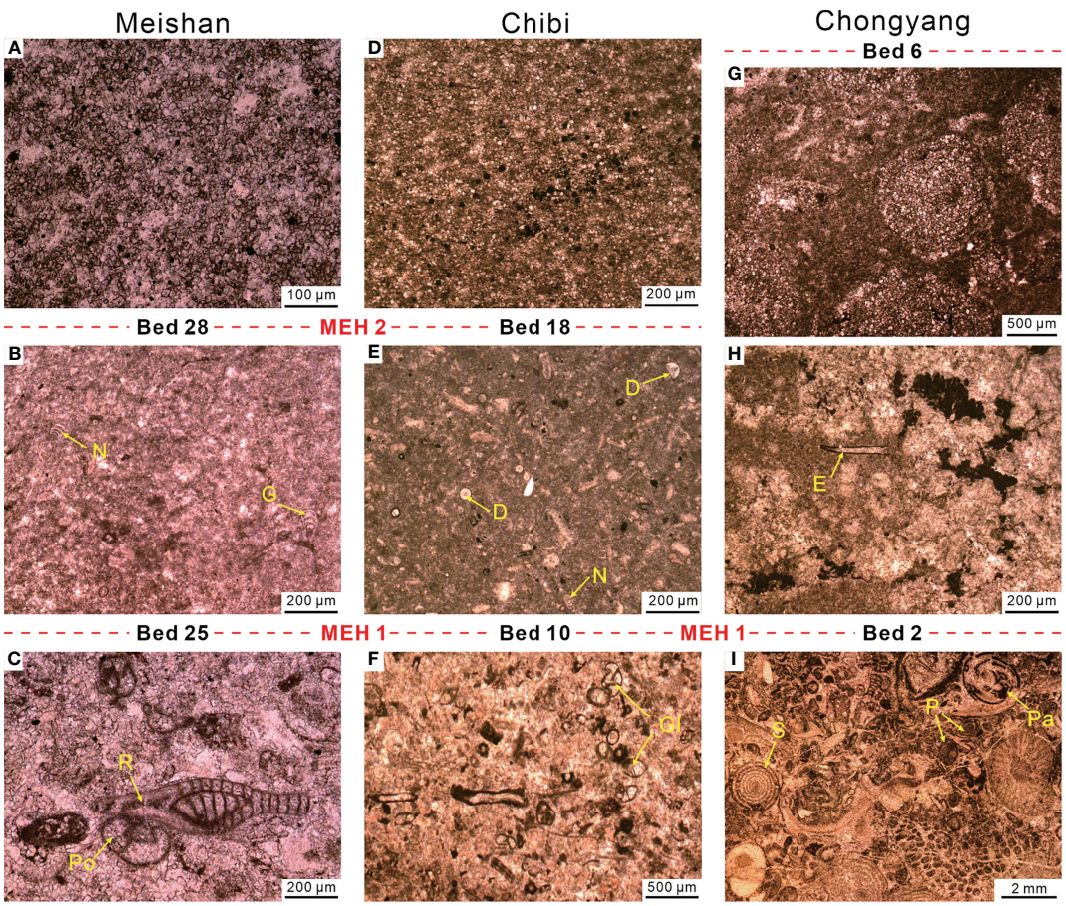

FIGURE 13 | Comparison of foraminifera features between Meishan **(A–C)**, Chibi **(D–F)**, and Chongyang **(G–I)** sections. **(A)** Micrite of Bed 29 with abundant pyrites but no fossil fragments. **(B)** Micrite of Bed 27a with few foraminifera. **(C)** Packstone of Bed 24, including abundant foraminifera and some algae fragments. **(D)** Marlstone of Bed 20 contains abundant pyrite. **(E)** Marlstone of Bed 13 contains few foraminifera. **(F)** Packstone of Bed 5 contains ca. 30% of algae and foraminifers. **(G)** Oolites of Bed 5. **(H)** Microbialite of Bed 3 containing few foraminifers and calcified cyanobacteria. **(I)** Grainstone of Bed 1, including over 80% bioclastic. D, *Diplosphaerina*; E, *Earlandia*; G, *Geinitzina*; Gl, *Globivalvulina*; N, *Nodosaria*; P, *Palaeofusulina*; Pa, *Paraglobivalvulina*; Po, *Poatendothyra*; R, *Reichelina*; S, *Sphaerulina*.

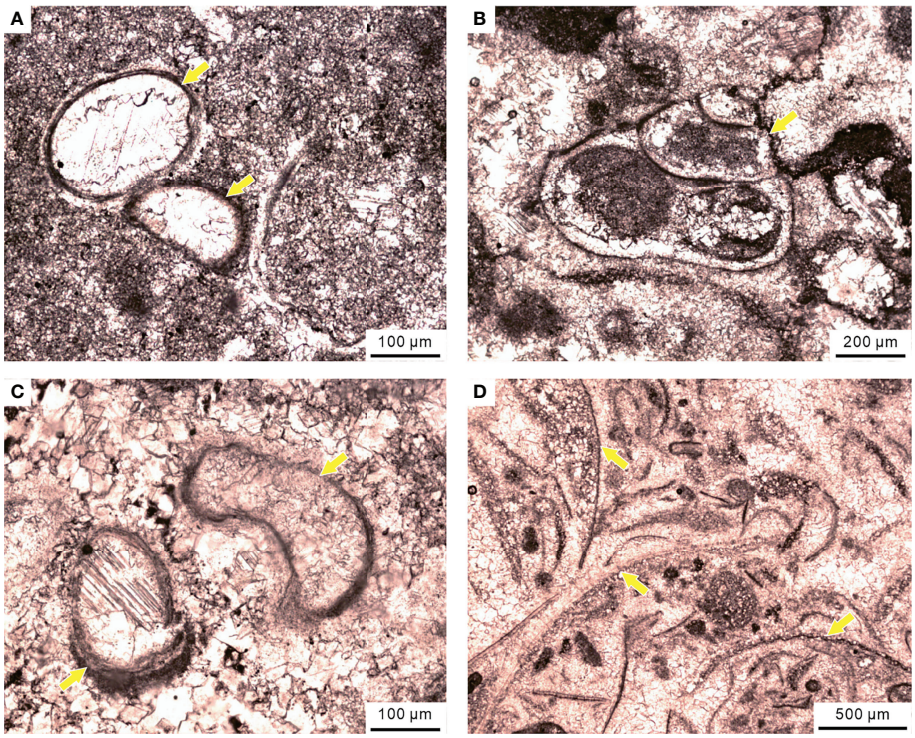

FIGURE 14 | Disaster forms in the MU of the Chongyang section during the PTME, including **(A)** ostracods, **(B)** small gastropods, **(C)** calcareous tubeworms, and **(D)** brachiopods.

foraminiferal diversity was substantially lower than that in Beds 1–9 before the first PTME pulse. Small foraminifers, such as *Earlandia*, *Geinitzina*, *Hemigoradius*, and *Nodosaria*, survived in the Chibi section (**Figures 10**, **13E**). The small foraminiferal assemblages from Beds 11–17 of the Chibi section were similar to those from P–Tr transition beds (Beds 25–27) of the Meishan section (**Figure 13B**; Song et al., 2009). It was worth noting that among the end-Permian foraminiferal assemblages, large-sized foraminifers disappeared in both Chongyang and Chibi sections after the first PTME pulse (**Figure 13**). Similarly, the large-sized foraminifers were also the most vulnerable victims of the first PTME pulse in the Liangfengya and Meishan sections (Song et al., 2007).

The bioclastic abundance dropped to less than 5% (**Figure 10A**), down from 20% or higher than this value in the Dalong Formation packstones (**Figure 6**). But the abundance of bioclastic from some samples of Beds 15–17 could reach or even exceeded the pre-extinction average, ca. 28% (**Figure 10B**). The second MEH (MEH 2) was located at the base of Bed 18, with disappearance of small-sized foraminifers *Diplosphaerina*, *Earlandia*, and *Nodosaria* (**Figure 13E**). The two-pulse extinction pattern of the Chibi section was similar to that in the Meishan section, i.e., the first pulse eliminated large-sized taxa with complex morphologies, and the second pulse chiefly affected the small ones (**Figure 13**). The two extinction pulses might be synchronous at the Chibi and Meishan sections, although this was less certain, for that we could not find well-preserved conodonts in the P–Tr boundary interval. Stratigraphic evidence (e.g., two claystone beds) and benthic assemblages suggested that the two extinction pulses in these two sections were synchronous.

5.3 Triggers of Migration and Extinction

5.3.1 Sea-Level and Sea Surface Temperature Changes

A correlation between global marine regressions and mass extinctions has been recognized since the last century, and sea-level fall was considered one of the prime causes of the events (Erwin, 1993; Gall et al., 1998). However, studies on numerous sections have called the generality of the regression–extinction relation into question (e.g., Hallam and Wignall, 1999; Baresel et al., 2017).

Seawater retreated from the Yangtze Platform at the end-Permian, reaching its lowest point in the *Clarkina meishanensis* and *Hindeodus changxingensis* zones (Yin et al., 2014), resulting in the absence of these two conodont zones and an ancient karst surface in most of the shallow-water platform. In shallow-water platforms of the SCB, Wu et al. (2010) pointed out that this hiatus was usually represented by concealed unconformity between the end-Permian limestone and the overlying MU, which coincided with *C. meishanensis* and *H. changxingensis* zones.

A sudden mass extinction pulse of benthos was recorded at the hiatus in the Chongyang section (**Figure 2**), and perhaps it was the hiatus of two conodont zones that had made the extinction seem more dramatic than it actually was. During the periods of drops in the sea level at the end-Permian (Yin et al., 2014), most of the shallow platform was exposed, and habitats of benthos were squeezed and fragmented. At the PTME interval, ca. 10°C rise of sea surface temperature (SST) was recorded in the tropics (Sun et al., 2012). Ocean warming has the potential to cause major shifts of planktonic distribution (Tarling et al., 2018). Overheating of surface waters during the PTB interval might result in extremely unsuitable habitats for shallow benthos. Climate modeling suggested that, in the tropics, water temperatures at 200-m depth were 10°C~12°C cooler than SST (Winguth et al., 2015).

In the context of global warming, the deep-ward migration of some shallow-water benthos was likely a more effective strategy than migration across the latitudes (Burrows et al., 2019). Thus, deeper waters might become a refuge for marine animals (Godbold et al., 2017). At the P–Tr transition, such extreme warming of SST could be a potentially potent driver for foraminifers to migrate to deeper and cooler waters. If an organism or population could not migrate, or when the rate of change exceeded its ability to do so, extinction was inevitable eventually. Mass extinctions might be related to shrunk habitats on shelves during severe regression (Newell, 1967; Fahrig, 2017). However, microfacies study revealed that the sea level of deeper-water sections was influenced slightly by the end-Permian major regression, so that foraminiferal diversity hotspot moved to the deeper-water slope (Liu et al., 2020).

The original exposed shallow platform was once again submerged by sea water and formed the MU succession during the Early Triassic transgression. The microfacies alterations of the MU reflected the early stages of the sea-level rise (Flügel, 2004). Some stratiform bioclastic grainstone layers were formed by small marine invertebrates in the MU of the Chongyang section. These invertebrates might have migrated from the original deeper-water slope during the sea-level rise and then bloomed in the shallow MU ephemerally as disaster forms (**Figure 14**).

Rapid high-amplitude regressive–transgressive couplets were frequent in the Earth's history (Miller et al., 2005), and most of them were not considered to be a probable cause of mass extinction (Hallam and Wignall, 1999). In short, sea-level change was a key driver of the migration between the platform and the slope but not the main trigger of mass extinction of marine benthos during the PTME interval.

5.3.2 Marine Euxinia/Anoxia

Widespread oceanic anoxia/euxinia (anoxic and sulfur-rich stratified ocean) shown by biomarkers (Grice et al., 2005), S-isotopic compositions (Riccardi et al., 2006), and pyrite framboid sizes (Wignall et al., 2005) has long been documented as a key trigger of the PTME (Isozaki, 1997; Grice et al., 2005; Meyer et al., 2008).

According to size distribution of pyrite framboids, Liao et al. (2010) indicated that the MU from the Laolongdong section grew in a lower dysoxic water column. The shallow-water anoxic event during the P–Tr transition has been considered to be the result of the expanding oxygen minimum zone (OMZ) (Algeo et al., 2010; Algeo and Twitchett, 2010). A recent study showed that the Northeast Pacific OMZ had expanded at a rate of 3.0 ± 0.7 m/year in the last 60 years and had lost 15% of its oxygen (Ross et al., 2020). Low oxygen levels could increase the dominance of benthos tolerant to anoxic conditions (Levin, 2003). For example, one foraminifer genus *Earlandia* flourished as the major "disaster form" in the MU after the first PTME pulse (**Figure 9A**) and probably migrated from the Chibi site during the Early Triassic transgression.

When compared to the Chongyang section, the decrease of algae abundance represented a decline in primary productivity, which might lead to the "dwarfism" of some consumers, e.g., foraminifera (Luo et al., 2006) and brachiopods (He et al., 2007). SEM was used to examine the samples from this stage, and no pyrite framboid was found in the two samples (**Table 1**), indicating that the water column contained a normal level of dissolved oxygen at that time (Bond and Wignall, 2010). This result was consistent with the paleomarine environment reflected by fossil assemblage and biogenic disturbance structure, in agreement with the "superanoxia" in the deep sea (Isozaki, 1997). In deep-water conditions, the dissolved oxygen level fluctuated, which could have induced reductions in the size of benthic foraminifers (Kaiho, 1998).

Another interesting feature was that those surviving foraminifers had a small size with simple morphology (**Figure 13**). For instance, *Nodosinelloides* had a mean volume value of ca. 6.2 log μm^3 in the end-Permian, which fell to 5.5 log μm^3 after the mass extinction (Song et al., 2011). The reduction in size and diversity of fauna with calcified skeletons have been linked to oxygen shortage in modern oceans (Byers, 1978; Levin, 2003). Laboratory experiments showed that the oxygen consumption rate increased significantly in foraminiferal specimens larger than 250 μm (Bradshaw, 1961). However, Luo et al. (2006) suggested that the size reduction of conodonts from the Meishan section was hardly related to anoxia. He et al. (2007) confirmed that there seemed to be no link between brachiopods shrinking and anoxic condition. Kaiho (1994) detected that benthic foraminifers were small-sized, thin-walled, and without sculpture if they inhabited in the lowered oxygen environment. Song et al. (2011) found that the anoxic event recorded in Bed 25 of the Meishan section coincided with the sharp reduction in foraminifer size. Therefore, Song et al. (2011) documented that small body sizes might have helped foraminifera to survive the mass extinction. The size distribution of pyrite framboids implied an anoxic bottom water in this study, while the foraminifera were smaller than pre-extinction foraminifer groups, particularly those extinction Permian groups (**Figure 13**). As a result, a relationship could be expected between anoxic conditions and the size reduction of the benthic foraminifers.

Wang et al. (2019) suggested that the increasing complexity in the benthic ecosystem might be related to hydrodynamic conditions of the Early Triassic transgression as revealed by texture and form of the MU. Our data showed another intriguing phenomenon that the metazoan assemblage in the MU of the

Chongyang section had good consistency with that in the Chibi section (**Figure 13**). This might shed light on transgression preceding the beginning of the Early Triassic, causing the metazoan to migrate from deep water to shallow platforms. A major increase in the δ^{13}C-depth gradient after the PTME suggested that deeper waters experienced more intense and prolonged oxygen restriction (Meyer et al., 2011).

Many layers of the MU contained calcified cyanobacteria (**Figure 9A**). Hypersalinity was one favorable chemical condition for the calcification of cyanobacteria (Pratt, 1984), which could inhibit ecological diversity of other organisms (Zhu et al., 1993). Most benthonic organisms tended to further reduce body size or diversity under high temperatures (Sun et al., 2012), anoxic water columns (Liao et al., 2010), and hypersalinity and intense evaporation (Zhu et al., 1993), whereas microbialite flourished in the shallow environment. This has led to a unique ecosystem dominated by "disaster forms" on shallow-water platforms of the SCB (**Figure 14**).

6 CONCLUSIONS

The PTME showed varied patterns among different paleogeographic sections. The shallow platform recorded one sudden extinction pulse at the topmost of the Changxing limestone, but the deeper-water slope suffered two pulses of marine extinction.

The end-Permian extensive regression caused the exposure of most shallow-marine platforms and then a sudden mass extinction. Sea level falls, extreme heat, and fragmented habitats led to the migration of some shallow-water benthos to deeper water at the same time.

During the Early Triassic transgression, some small foraminifers migrated from the slopes to the shallow platforms. A unique ecosystem has been rebuilt on shallow water platforms of the SCB due to high temperatures, strong evaporation, and hypersalinity after the first PTME pulse.

Pyrite framboid size distributions showed that oceanic anoxia was likely an important trigger contributing to the deeper-water benthic extinction. The abundant small pyrite framboids in the P–Tr transition beds suggested that the redox conditions of the bottom water changed immediately from oxic to anoxic after the MEH 1. Size distributions of these samples indicated that the bottom waters had a fluctuation between anoxic and upper dysoxic during the mass extinction. Pyrite framboid parameters indicated that oxygen deficiency in the bottom water was intensified and stable at anoxia after the second PTME pulse.

DATA AVAILABILITY STATEMENT

The original contributions presented in the study are included in the article/supplementary material. Further inquiries can be directed to the corresponding authors.

AUTHOR CONTRIBUTIONS

GL, YW, SL, TW, WL, and BD collected the samples and photographs in the field. GL, TW, and SL carried out the laboratory measurements and data analysis. YW supervised the data analysis. GL and ZL created the figures and wrote the article. All authors contributed to the ideas and final article.

ACKNOWLEDGMENTS

This study was jointly supported by the National Natural Science Foundation of China (Grant No. 41730320 and No. 41962003), Innovation and Entrepreneurship Project of Shantou (201112176541391), and STU Scientific Research Start-Up Foundation for Talents (NTF19003). Thanks are due to Dr. Rashid Pervez for polishing the language.

REFERENCES

Aberhan, M., and Kiessling, W. (2015). Persistent Ecological Shifts in Marine Molluscan Assemblages Across the End-Cretaceous Mass Extinction. *Proc. Natl. Acad. Sci. U.S.A.* 112, 7207–7212. doi: 10.1073/pnas.1422248112

Algeo, T. J., Chen, Z. Q., Fraiser, M. L., and Twitchett, R. J. (2011). Terrestrial–marine Teleconnections in the Collapse and Rebuilding of Early Triassic Marine Ecosystems. *Palaeogeogr. Palaeoclimatol. Palaeoecol.* 308, 1–11. doi: 10.1016/j.palaeo.2011.01.011

Algeo, T. J., Hinnov, L., Moser, J., Maynard, J. B., Elswick, E., Kuwahara, K., et al. (2010). Changes in Productivity and Redox Conditions in the Panthalassic Ocean During the Latest Permian. *Geology* 38 (2), 187–190. doi: 10.1130/G30483.1

Algeo, T. J., and Twitchett, R. J. (2010). Anomalous Early Triassic Sediment Fluxes Due to Elevated Weathering Rates and Their Biological Consequences. *Geology* 38 (11), 1023–1026. doi: 10.1130/G31203.1

Angiolini, L., Checconi, A., Gaetani, M., and Rettori, R. (2010). The Latest Permian Mass Extinction in the Alborz Mountains (North Iran). *Geol. J.* 45 (2–3), 216–229. doi: 10.1002/gj.1203

Baresel, B., Bucher, H., Bagherpour, B., Brosse, M., Guodun, K., and Schaltegger, U. (2017). Timing of Global Regression and Microbial Bloom Linked With the Permian-Triassic Boundary Mass Extinction: Implications for Driving Mechanisms. *Sci. Rep.* 7 (1), 1–8. doi: 10.1038/srep43630

Benton, M. J., and Newell, A. J. (2014). Impacts of Global Warming on Permo-Triassic Terrestrial Ecosystems. *Gondwana. Res.* 25, 1308–1337. doi: 10.1016/j.gr.2012.12.010

Black, B. A., Elkins-Tanton, L. T., Rowe, M. C., and Peate, I. U. (2012). Magnitude and Consequences of Volatile Release From the Siberian Traps. *Earth Planet. Sci. Lett.* 317-318, 363–373. doi: 10.1016/j.epsl.2011.12.001

Bond, D. P. G., and Wignall, P. B. (2010). Pyrite Framboid Study of Marine Permian–Triassic Boundary Sections: A Complex Anoxic Event and its Relationship to Contemporaneous Mass Extinction. *Geological. Soc. America Bull.* 122 (7-8), 1265–1279. doi: 10.1130/B30042.1

Bradshaw, J. S. (1961). Laboratory Experiments on the Ecology of Foraminifera. *Cushman. Found. Foram. Res. Contr.* 17, 87–106.

Breitburg, D., Levin, L. A., Oschlies, A., Grégoire, M., Chavez, F. P., Conley, D. J., et al. (2018). Declining Oxygen in the Global Ocean and Coastal Waters. *Science* 359 (6371), eaam7240. doi: 10.1126/science.aam7240

Burgess, S. D., Muirhead, J. D., and Bowring, S. A. (2017). Initial Pulse of Siberian Traps Sills as the Trigger of the End-Permian Mass Extinction. *Nat. Commun.* 8, 164–169. doi: 10.1038/s41467-017-00083-9

Burrows, M. T., Bates, A. E., Costello, M. J., Edwards, M., Edgar, G. J., Fox, C. J., et al. (2019). Ocean Community Warming Responses Explained by Thermal Affinities and Temperature Gradients. *Nat. Clim. Change* 9 (12), 959–963. doi: 10.1038/s41558-019-0631-5

Byers, C. W. (1978). Biofacies Patterns in Euxinic Basins: A General Model. *Special. Publ. – Soc. Economic. Paleontol. Mineral.* 25, 5–17. doi: 10.2110/pec.77.25.005

Ceballos, G., and Ehrlich, P. R. (2018). The Misunderstood Sixth Mass Extinction. *Science* 360 (6393), 1080–1081. doi: 10.1126/science.aau0191

Ceballos, G., Ehrlich, P. R., and Dirzo, R. (2017). Biological Annihilation *via* the Ongoing Sixth Mass Extinction Signaled by Vertebrate Population Losses and Declines. *Proc. Natl. Acad. Sci.* 114 (30), 6089–6096. doi: 10.1073/pnas.1704949114

Chen, Z. Q., and Benton, M. J. (2012). The Timing and Pattern of Biotic Recovery Following the End-Permian Mass Extinction. *Nat. Geosci.* 5 (6), 375–383. doi: 10.1038/ngeo1475

Chen, Z. Q., Yang, H., Luo, M., Benton, M. J., Kaiho, K., Zhao, L., et al. (2015). Complete Biotic and Sedimentary Records of the Permian–Triassic Transition From Meishan Section, South China: Ecologically Assessing Mass Extinction and its Aftermath. *Earth-Sci. Rev.* 149, 67–107. doi: 10.1016/j.earscirev.2014.10.005

Chivas, A. R., Torgersen, T., and Polach, H. A. (1990). Growth Rates and Holocene Development of Stromatolites From Shark Bay, Western Australia. *Aust. J. Earth Sci.* 37 (2), 113–121. doi: 10.1080/08120099008727913

Clarkson, M. O., Kasemann, S. A., Wood, R. A., Lenton, T. M., Daines, S. J., Richoz, S., et al. (2015). Ocean Acidification and the Permo-Triassic Mass Extinction. *Science* 348 (6231), 229–232. doi: 10.1126/science.aaa0193

Cowie, R. H., Bouchet, P., and Fontaine, B. (2022). The Sixth Mass Extinction: Fact, Fiction or Speculation? *Biol. Rev.* 97 (2), 640–663. doi: 10.1111/brv.12816

Dal, C. J., Song, H., Callegaro, S., Chu, D., Sun, Y., Hilton, J., et al. (2022). Environmental Crises at the Permian–Triassic Mass Extinction. *Nat. Rev. Earth Environ.* 3, 1–18. doi: 10.1038/s43017-021-00259-4

Deng, B., Yu, L., Wang, Y., Li, G., and Meng, Y. (2015). Evolution of Marine Conditionsand Sedimentation During the Permian-Triassic Transition in Chibi of Hubei Province (in Chinese With English Abstract). *Earth Sci. - J. China Univ. Geosci.* 40, 317–326. doi: 10.3799/dqkx.2015.024

Diaz, M. R., Swart, P. K., Eberli, G. P., Oehlert, A. M., Devlin, Q., Saeid, A., et al. (2015). Geochemical Evidence of Microbial Activity Within Ooids. *Sedimentology* 62, 2090–2112. doi: 10.1111/sed.12218

Erwin, D. H. (1993). *The Great Paleozoic Crisis: Life and Death in the Permian* (New York: ColumbiaUniv. Press), 327 pp.

Erwin, D. H., Bowring, S. A., and Yugan, J. (2002). End-Permian Mass Extinctions: A Review. *Special. Papers-Geological. Soc. America* 356, 363–383. doi: 10.1130/0-8137-2356-6.363

Ezaki, Y., Liu, J., and Adachi, N. (2003). Earliest Triassic Microbialite Micro-to Megastructures in the Huaying Area of Sichuan Province, South China: Implications for the Nature of Oceanic Conditions After the End-Permian Extinction. *Palaios* 18 (4-5), 388–402. doi: 10.1669/0883-1351(2003)018<0388:ETMMTM>2.0.CO;2

Fahrig, L. (2017). Ecological Responses to Habitat Fragmentation Per Se. *Annu. Rev. Ecol. Evol. Syst.* 48, 1–23. doi: 10.1146/annurev-ecolsys-110316-022612

Fan, J. X., Shen, S. Z., Erwin, D. H., Sadler, P. M., MacLeod, N., Cheng, Q. M., et al. (2020). A High-Resolution Summary of Cambrian to Early Triassic Marine Invertebrate Biodiversity. *Science* 367 (6475), 272–277. doi: 10.1126/science.aax4953

Feng, Z. Z., Yang, Y. Q., Jin, Z. K., He, Y. B., Wu, S. H., Xin, W. J., et al. (1996). Lithofacies Paleogeography of the Permian of South China. *Acta Sedimentol. Sin.* 14, 1–11. doi: 10.14027/j.cnki.cjxb.1996.02.001

Flügel, E. (2004). Microfacie of Carbonate Rocks: Analysis, Interpretation and Application, Berlin-Heidelberg. *Springer-Verlag*, 680–724. pp.

Forel, M.-B. (2013). The Permian–Triassic Mass Extinction: Ostracods (Crustacea) and Microbialites. *Compt. Rendus. Geosci.* 345 (4), 203–211. doi: 10.1016/j.crte.2013.03.003

Foster, W. J., Lehrmann, D. J., Yu, M., and Martindale, R. C. (2019). Facies Selectivity of Benthic Invertebrates in a Permian/Triassic Boundary Microbialite Succession: Implications for the "Microbialite Refuge" Hypothesis. *Geobiology* 17, 523–535. doi: 10.1111/gbi.12343

Gall, J. C., Grauvogel-Stamm, L., Nel, A., and Papier, F. (1998). The Permian Mass Extinction and the Triassic Recovery. *Comptes. Rendus. l'Academie. Des. Sci. Ser. IIA. Earth Planet. Sci.* 1 (326), 1–12.

Godbold, A., Schoepfer, S., Shen, S., and Henderson, C. M. (2017). Precarious Ephemeral Refugia During the Earliest Triassic. *Geology* 45 (7), 607–610. doi: 10.1130/G38793.1

Grice, K., Cao, C., Love, G. D., Bottcher, M. E., Twitchett, R. J., Grosjean, E., et al. (2005). Photic Zone Euxinia During the Permian–Triassic Superanoxic Event. *Science* 307, 706–709. doi: 10.1126/science.1104323

Groves, J., Altiner, D., and Rettori, R. (2005). Extinction, Survival, and Recovery of Lagenide Foraminifers in the Permian–Triassic Boundary Interval, Central Taurides, Turkey. *J. Paleontol.* 79, 1–39. doi: 10.1666/0022-3360(2005)79[1:ESAROL]2.0.CO;2

Groves, J. R., Payne, J. L., and Altiner, D. (2007). End-Permian Mass Extinction of Lagenide Foraminifers in the Southern Alps (Northern Italy). *J. Paleontol.* 81 (3), 415–434. doi: 10.1666/05123.1

Hallam, A., and Wignall, P. B. (1997). *Mass Extinctions and Their Aftermath* (UK: Oxford University Press).

Hallam, A., and Wignall, P. B. (1999). Mass Extinctions and Sea-Level Changes. *Earth-Sci. Rev.* 48 (4), 217–250. doi: 10.1016/S0012-8252(99)00055-0

Harris, P., Diaz, M. R., and Eberli, G. P. (2019). The Formation and Distribution of Modern Ooids on Great Bahama Bank. *Annu. Rev. Marine. ence.* 11 (1), 491–516. doi: 10.1146/annurev-marine-010318-095251

He, W., Shi, G. R., Feng, Q., Campi, M. J., Gu, S., and Bu, J. (2007). Brachiopod Miniaturization and its Possible Causes During the Permian-Triassic Crisis in Deep Water Environments, South China. *Palaeogeograp. Palaeoclimatol. Palaeoecol.* 252 (1-2), 145–163. doi: 10.1016/j.palaeo.2006.11.040

He, W. H., Twitchett, R. J., Zhang, Y., Shi, G. R., Feng, Q. L., Yu, J. X., et al. (2010). Controls on Body Size During the Late Permian Mass Extinction Event. *Geobiology* 8, 391–402. doi: 10.1111/j.1472-4669.2010.00248.x

Hülse, D., Lau, K. V., van de Velde, S. J., Arndt, S., Meyer, K. M., and Ridgwell, A. (2021). End-Permian Marine Extinction Due to Temperature-Driven Nutrient Recycling and Euxinia. *Nat. Geosci.* 14 (11), 862–867. doi: 10.1038/s41561-021-00829-7

Ishida, H., Isono, R. S., Kita, J., and Watanabe, Y. W. (2021). Long-Term Ocean Acidification Trends in Coastal Waters Around Japan. *Sci. Rep.* 11 (1), 1–7. doi: 10.1038/s41598-021-84657-0

Isozaki, Y. (1997). Permo-Triassic Boundary Superanoxia and Stratified Superocean: Records From Lost Deep Sea. *Science* 276, 235–238. doi: 10.1126/science.276.5310.235

Jiang, H., Lai, X., Sun, Y., Wignall, P. B., Liu, J., and Yan, C. (2014). Permian-Triassic Conodonts From Dajiang (Guizhou, South China) and Their Implication for the Age of Microbialite Deposition in the Aftermath of the End-Permian Mass Extinction. *J. Earth Sci.* 25, 413–430. doi: 10.1007/s12583-014-0444-4

Jin, Y. G., Wang, Y., Wang, W., Shang, Q. H., Cao, C. Q., and Erwin, D. H. (2000). Pattern of Marine Mass Extinction Near the Permian-Triassic Boundary in South China. *Science* 289, 432–436. doi: 10.1126/science.289.5478.432

Joachimski, M. M., Alekseev, A. S., Grigoryan, A., and Gatovsky, Y. A. (2019). Siberian Trap Volcanism, Global Warming and the Permian-Triassic Mass Extinction: New Insights From Armenian Permian-Triassic Sections. *GSA Bull.* 132, 427–443. doi: 10.1130/B35108.1

Kaiho, K. (1994). Benthic Foraminiferal Dissolved-Oxygen Index and Dissolved-Oxygen Levels in the Modern Ocean. *Geology* 22 (8), 719–722. doi: 10.1130/0091-7613(1994)022<0719:BFDOIA>2.3.CO;2

Kaiho, K. (1998). Global Climatic Forcing of Deep-Sea Benthic Foraminiferal Test Size During the Past 120 M.Y. *Geology* 26, 491–494. doi: 10.1130/0091-7613(1998)026<0491:GCFODS>2.3.CO;2

Kaiho, K., Aftabuzzaman, M., Jones, D. S., and Tian, L. (2020). Pulsed Volcanic Combustion Events Coincident With the End-Permian Terrestrial Disturbance and the Following Global Crisis. *Geology* 49, 289–293. doi: 10.1130/G48022.1

Kershaw, S., Crasquin, S., Li, Y., Collin, P., Forel, M., Mu, X., et al. (2012). Microbialites and Global Environmental Change Across the Permian–Triassic

Boundary: A Synthesis. *Geobiology* 10, 25–47. doi: 10.1111/j.1472-4669.2011.00302.x

Levin, L. A. (2003). "Oxygen Minimum Zone Bethos: Adaptation and Community Response to Hypoxia," in *Oceanography and Marine Biology. An Annual Review*, vol. 41 . Eds. R. N. Gibson and R. J. A. Atkinson, (Boca Raton: CRC Press) 1–45 pp.

Liao, W., Wang, Y., Kershaw, S., Weng, Z., and Hao, Y. (2010). Shallow-Marine Dysoxia Across the Permian–Triassic Boundary: Evidence From Pyrite Framboids in the Microbialite in South China. *Sediment. Geol.* 232 (1-2), 77–83. doi: 10.1016/j.sedgeo.2010.09.019

Li, G., Liao, W., Li, S., Wang, Y., and Lai, Z. (2021). Different Triggers for the Two Pulses of Mass Extinction Across the Permian and Triassic Boundary. *Sci. Rep.* 11, 6686. doi: 10.1038/s41598-021-86111-7

Liu, X., Song, H., Bond, D. P. G., Tong, J., and Benton, M. J. (2020). Migration Controls Extinction and Survival Patterns of Foraminifers During the Permian-Triassic Crisis in South China. *Earth-Sci. Rev.* 209, 103329. doi: 10.1016/j.earscirev.2020.103329

Liu, H., Wang, Y., Yuan, A., Yang, H., Song, H., and Zhang, S. (2010). Ostracod Fauna Across the Permian-Triassic Boundary at Chongyang, Hubei Province, and its Implication for the Process of the Mass Extinction. *Sci. China Earth Sci.* 53, 810–817. doi: 10.1007/s11430-010-0045-8

Luo, G., Lai, X., Jiang, H., and Zhang, K. (2006). Size Variation of the End Permian Conodont Neogondolella at Meishan Section, Changxing, Zhejiang and its Significance. *Sci. China Ser. D* 49, 337–347. doi: 10.1007/s11430-006-0337-1

Meng, Z., Wang, Y. B., Woods, A., Liao, W., and Li, G. S. (2014). Deep Shelf Biostrome of Late Permian in South China and its Implications for the Adaptability of Calcisponges to Water Depth. *Palaeogeogr. Palaeoclimatol. Palaeoecol.* 401, 132–141. doi: 10.1016/j.palaeo.2014.02.028

Meyer, K. M., Kump, L. R., and Ridgwell, A. (2008). Biogeochemical Controls on Photic-Zone Euxinia During the End-Permian Mass Extinction. *Geology* 36, 747–750. doi: 10.1130/G24618A.1

Meyer, K. M., Yu, M., Jost, A. B., Kelley, B. M., and Payne, J. L. (2011). ä13C Evidence that High Primary Productivity Delayed Recovery from End-Permian Massextinction. *Earth Planetary Science Letters* 302 (3-4), 378–384. doi: 10.1016/j.epsl.2010.12.033

Miller, K. G., Kominz, M. A., Browning, J. V., Wright, J. D., Mountain, G. S., Katz, M. E., et al. (2005). The Phanerozoic Record of Global Sea-Level Change. *Science* 310 (5752), 1293–1298.

Newell, N. D. (1967). Revolutions in the History of Life. *Geol. Soc Am. Spec. Pap.* 89, 63–91. doi: 10.1130/SPE89-p63

O'Reilly, S. S., Mariotti, G., Winter, A. R., Newman, S. A., Matys, E. D., McDermott, F., et al. (2017). Molecular Biosignatures Reveal Common Benthic Microbial Sources of Organic Matter in Ooids and Grapestones From Pigeon Cay, the Bahamas. *Geobiology* 15, 112–130. doi: 10.1111/gbi.12196

Payne, J. L., Lehrmann, D. J., Wei, J., and Knoll, A. H. (2006). The Pattern and Timing of Biotic Recovery From the End-Permian Extinction on the Great Bank of Guizhou, Guizhou Province, China. *Palaios* 21, 63–85. doi: 10.2110/palo.2005.p05-12p

Payne, J. L., Turchyn, A. V., Paytan, A., Depaolo, D. J., Lehrmann, D. J., Yu, M., et al. (2010). Calcium Isotope Constraints on the End-Permian Mass Extinction. *Proc. Natl. Acad. Sci. U. S. A.* 107 (19), 8543–8548. doi: 10.1073/pnas.0914065107

Peng, Y. Q., and Tong, J. N. (1999). Integrated Study on Permian-Triassic Boundary Bed Inyangtze Platform. *Earth Sci.* 24 (1), 39–48.

Pimm, S. L., Jenkins, C. N., Abell, R., Brooks, T. M., Gittleman, J. L., Joppa, L. N., et al. (2014). The Biodiversity of Species and Their Rates of Extinction, Distribution, and Protection. *Science* 344, 6187. doi: 10.1126/science.1246752

Pratt, B. R. (1984). Epiphyton and Renalcis-Diagenetic Microfossils From Calcification of Coccoid Blue-Green Algae. *J. Sediment. Petrol.* 54, 948–971.

Raup, D. M., and Sepkoski, J. J.Jr. (1982). Mass Extinctions in the Marine Fossil Record. *Science* 215, 1501–1503. doi: 10.1126/science.215.4539.1501

Reid, R. P., Macintyre, I. G., Browne, K. M., Steneck, R. S., and Miller, T. (1995). Modern Marine Stromatolites in the Exuma Cays, Bahamas: Uncommonly Common. *Facies* 33 (1), 1–17. doi: 10.1007/BF02537442

Riccardi, A. L., Arthur, M. A., and Kump, L. R. (2006). Sulfur Isotopic Evidence for Chemocline Upward Excursions During the End-Permian Mass Extinction. *Geochim. Cosmochim. Acta* 70 (23), 5740–5752. doi: 10.1016/j.gca.2006.08.005

Rong, J., and Fang, Z. (2004). *Mass Extinction and Recovery: Evicences From the Palaeozoic and Triassic of South China* (Hefei: University of Science and Technology of China Press).

Ross, T., Du Preez, C., and Ianson, D. (2020). Rapid Deep Ocean Deoxygenation and Acidification Threaten Life on Northeast Pacific Seamounts. *Global Change Biol.* 26 (11), 6424–6444. doi: 10.1111/gcb.15307

Ruban, D. A. (2020). Paleozoic–Mesozoic Eustatic Changes and Mass Extinctions: New Insights From Event Interpretation. *Life* 10 (11), 281. doi: 10.3390/life10110281

Scotese, C. R. (2001). *Atlas of Earth History* (Texas: University of Texas at Arlington, Department of Geology. PALEOMAP Project), 58 pp.

Seager, R., Cane, M., Henderson, N., Lee, D. E., Abernathey, R., and Zhang, H. (2019). Strengthening Tropical Pacific Zonal Sea Surface Temperature Gradient Consistent With Rising Greenhouse Gases. *Nat. Climate Change* 9 (7), 517–522. doi: 10.1038/s41558-019-0505-x

Sepkoski, J. J. (1986). "Phanerozoic Overview of Mass Extinction," in *Patterns and Processes in the History of Life. Dahlem Workshop Reports*, vol. vol 36 . Eds. D. M. Raup and D. Jablonski (Berlin, Heidelberg: Springer), 277–295. doi: 10.1007/978-3-642-70831-2_15

Shen, S. Z., Cao, C. Q., Henderson, C. M., Wang, X. D., Shi, G. R., Wang, Y., et al. (2006). End-Permian Mass Extinction Pattern in the Northern Peri-Gondwanan Region. *Palaeoworld* 15 (1), 3–30. doi: 10.1016/j.palwor.2006.03.005

Shen, S. Z., Crowley, J. L., Wang, Y., Bowring, S. A., Erwin, D. H., Sadler, P. M., et al. (2011). Calibrating the End-Permian Mass Extinction. *Science* 334, 1367–1372. doi: 10.1126/science.1213454

Song, H., Tong, J., and Chen, Z. Q. (2009). Two Episodes of Foraminiferal Extinction Near the Permian–Triassic Boundary at the Meishan Section, South China. *Aust. J. Earth Sci.* 56, 765–773. doi: 10.1080/08120090903002599

Song, H., Tong, J., and Chen, Z. Q. (2011). Evolutionary Dynamics of the Permian–Triassic Foraminifer Size: Evidence for Lilliput Effect in the End-Permian Mass Extinction and its Aftermath. *Palaeogeograp. Palaeoclimatol. Palaeoecol.* 308 (1-2), 98–110. doi: 10.1016/j.palaeo.2010.10.036

Song, H. J., Tong, J. N., Zhang, K. X., Wang, Q. X., and Chen, Z. Q. (2007). Foraminiferal Survivors From the Permian-Triassic Mass Extinction in the Meishan Section, South China. *Palaeoworld* 16, 105–119. doi: 10.1016/j.palwor.2007.05.016

Song, H., Wignall, P. B., and Dunhill, A. M. (2018). Decoupled Taxonomic and Ecological Recoveries From the Permo-Triassic Extinction. *Sci. Adv.* 4 (10), eaat5091. doi: 10.1126/sciadv.aat5091

Song, H., Wignall, P. B., Tong, J., and Yin, H. (2012). Two Pulses of Extinction During the Permian–Triassic Crisis. *Nat. Geosci.* 6, 52–56. doi: 10.1038/ngeo1649

Stanley, S., and Yang, X. (1994). A Double Mass Extinction at the End of the Paleozoic Era. *Science* 266 (5189), 1340–1344.

Sun, Y., Joachimski, M. M., Wignall, P. B., Yan, C., Chen, Y., Jiang, H., et al. (2012). Lethally Hot Temperatures During the Early Triassic Greenhouse. *Science* 338, 366–370. doi: 10.1126/science.1224126

Tarling, G. A., Ward, P., and Thorpe, S. E. (2018). Spatial Distributions of Southern Ocean Mesozooplankton Communities Have Been Resilient to Long-Term Surface Warming. *Global Change Biol.* 24 (1), 132–142. doi: 10.1111/gcb.13834

Wang, T., Burne, R. V., Yuan, A. H., Wang, Y. B., and Yi, Z. X. (2019). The Evolution of Microbialite Forms During the Early Triassic Transgression: A Case Study in Chongyang of Hubei Province, South China. *Palaeogeogr. Palaeoclimatol. Palaeoecol.* 519, 209–220. doi: 10.1016/j.palaeo.2018.01.043

Wang, Y., and Jin, Y. (2000). Permian Palaeogeographic Evolution of the Jiangnan Basin, South China. *Palaeogeogr. Palaeoclimatol. Palaeoecol.* 160, 35–44. doi: 10.1016/S0031-0182(00)00043-2

Wang, Y., Tong, J., Wang, J., and Zhou, X. (2005). Calcimicrobialite After End-Permian Mass Extinction in South China and its Pa-Laeoenvironmental Signifi-Cance. *Chin. Sci. Bull.* 50, 665–671. doi: 10.1360/982004-323

Wang, L., Wignall, P. B., Wang, Y., Jiang, H., Sun, Y., Li, G., et al. (2016). Depositional Conditions and Revised Age of the Permo-Triassic Microbialites at Gaohua Section, Cili County (Hunan Province, South China). *Palaeogeograp. Palaeoclimatol. Palaeoecol.* 443, 156–166. doi: 10.1016/j.palaeo.2015.11.032

Wang, G. Q., and Xia, W. C. (2003). The Changhsingian Conodont Zonation and Variation of Organic Carbon Isotope of Huangshi Ermen Section, Hubei Province. *Geoscience* 04, 378–386.

Wan, J., Yuan, A., Crasquin, S., Jiang, H., Yang, H., and Hu, X. (2019). High-Resolution Variation in Ostracod Assemblages From Microbialites Near the Permian-Triassic Boundary at Zuodeng, Guangxi Region, South China. *Palaeogeogr. Palaeoclimatol. Palaeoecol.* 535, 109349. doi: 10.1016/j.palaeo.2019.109349

Wen, J., and Liu, J. (2009). Quantitative Study of Bioclastic Grains in Carbonate Rocks: Theoretical Analysis and Application of Point-Counting Method. *J. Palaeogeogr.* 11, 581–592.

Wignall, P. B., and Hallam, A. (1996). Facies change and the end-Permian mass extinction in SE Sichuan, China. *Palaios* 587–596. doi: 10.2307/3515193

Wignall, P. B., Newton, R., and Brook field, M. E. (2005). Pyrite Framboid Evidence for Oxygenpoor Deposition During the Permian–Triassic Crisis in Kashmir. *Palaeogeogr. Palaeoclimatol. Palaeoecol.* 216, 183–188. doi: 10.1016/j.palaeo.2004.10.009

Wilkin, R. T., Barnes, H. L., and Brantley, S. L. (1996). The Size Distribution of Framboidal Pyrite in Modern Sediments: An Indicator of Redox Conditions. *Geochim. Cosmochim. Acta* 60, 3897–3912. doi: 10.1016/0016-7037(96)00209-8

Winguth, A. M., Shields, C. A., and Winguth, C. (2015). Transition Into a Hothouse World at the Permian–Triassic Boundary—a Model Study. *Palaeogeograp. Palaeoclimatol. Palaeoecol.* 440, 316–327. doi: 10.1016/j.palaeo.2015.09.008

Wu, Y. S., Jiang, H. X., and Fan, J. S. (2010). Evidence for Sea-Level Falls in the Permian-Triassic Transition in the Ziyun Area, South China. *Geological. J.* 45 (2–3), 170–185.

Wu, Y. S., Jiang, H. X., and Liao, T. P. (2006). Sea-Level Drops in the Permian-Triassic Boundary Section at Laolongdong, Chongqing, Sichuan Province. *Acta Petrologica. Sin.* 22 (9), 2405–2412.

Xie, S., Pancost, R. D., Yin, H., Wang, H., and Evershed, R. P. (2005). Two Episodes of Microbial Change Coupled With Permo/Triassic Faunal Mass Extinction. *Nature* 434 (7032), 494–497. doi: 10.1038/nature03396

Yang, H., Chen, Z. Q., Wang, Y., Tong, J., Song, H., and Chen, J. (2011). Composition and Structure of Microbialite Ecosystems Following the End-Permian Mass Extinction in South China. *Palaeogeogr. Palaeoclimatol. Palaeoecol.* 308, 111–128. doi: 10.1016/j.palaeo.2010.05.029

Yang, H., Zhang, S. X., Jiang, H. S., and Wang, Y. B. (2006). Age and General Characteristics of the Calimicrobialite Near the Permian-Triassic Boundary in Chongyang, Hubei Province. *J. China Univ. Geosci.* 17, 121–125. doi: 10.1016/S1002-0705(06)60016-2

Yin, H., Feng, Q., Lai, X., Baud, A., and Tong, J. (2007). The Protracted Permo-Triassic Crisis and Multi-Episode Extinction Around the Permian–Triassic Boundary. *Global Planet. Change* 55, 1–20. doi: 10.1016/j.gloplacha.2006.06.005

Yin, H., Jiang, H., Xia, W., Feng, Q., Zhang, N., and Shen, J. (2014). The End-Permian Regression in South China and its Implication on Mass Extinction. *Earth-Sci. Rev.* 137, 19–33. doi: 10.1016/j.earscirev.2013.06.003

Yin, H., and Song, H. (2013). Mass Extinction and Pangea Integration During the Paleozoic-Mesozoic Transition. *Sci. China Earth Sci.* 56, 1791–1803. doi: 10.1007/s11430-013-4624-3

Yin, H., Zhang, K., Tong, J., Yang, Z., and Wu, S. (2001). The Global Stratotype Section and Point (GSSP) of the Permian-Triassic Boundary. *Episodes* 24, 102–114. doi: 10.18814/epiiugs/2001/v24i2/004

Yu, S. Y. (1989). *Fossils Carbonates Microfacies* (Beijing: Geological Publishing House).

Yu, J. X., Broutin, J., Chen, Z. Q., Shi, X., Li, H., Chu, D. L., et al. (2015). Vegetation Changeover Across the Permian–Triassic Boundary in Southwest China Extinction, Survival, Recovery and Palaeoclimate: A Critical Review. *Earth Sci. Rev.* 149, 203–224. doi: 10.1016/j.earscirev.2015.04.005

Zhang, M., and Gu, S. (2015). Latest Permian Deep-Water Foraminifers From Daxiakou, Hubei, South China. *J. Paleontol.* 89 (3), 448–464. doi: 10.1017/jpa.2015.19

Zhu, Z., Kuang, H., Liu, Y., Benton, M. J., Newell, A. J., Xu, H., et al. (2020). Intensifying Aeolian Activity Following the End-Permian Mass Extinction: Evidence From the Late Permian–Early Triassic Terrestrial Sedimentary Record of the Ordos Basin, North China. *Sedimentology* 67 (5), 2691–2720. doi: 10.1111/sed.12716

Zhu, S., Liang, Y., and Du, R. (1993). *The Stromatolites of China* (Tianjin: Tianjin University Press), 191–196.

Conflict of Interest: The authors declare that the research was conducted in the absence of any commercial or financial relationships that could be construed as a potential conflict of interest.

Publisher's Note: All claims expressed in this article are solely those of the authors and do not necessarily represent those of their affiliated organizations, or those of the publisher, the editors and the reviewers. Any product that may be evaluated in this article, or claim that may be made by its manufacturer, is not guaranteed or endorsed by the publisher.